JGR Space Physics

RESEARCH ARTICLE
10.1029/2020JA028044

Comparison of Quality Measures for Walén Relation

G. Paschmann[1], B. U. Ö. Sonnerup[2], S. E. Haaland[3,4], T.-D. Phan[5], and R. E. Denton[6]

[1]Max-Planck-Institut für extraterrestrische Physik, Garching, Germany, [2]Thayer School of Engineering, Dartmouth College, Hanover, NH, USA, [3]Birkeland Centre for Space Science, University of Bergen, Bergen, Norway, [4]Max-Planck-Institut für Sonnensystemforschung, Göttingen, Germany, [5]Space Sciences Laboratory, University of California, Berkeley, CA, USA, [6]Department of Physics and Astronomy, Dartmouth College, Hanover, NH, USA

Key Points:
- Statistical results from different versions of the Walén test are compared, using MMS data at the dayside magnetopause
- The quality measures should employ significantly different acceptance threshold values to identify rotational discontinuities
- Relationships between the various quality measures are explored and quantified

Correspondence to:
G. Paschmann,
goetz.paschmann@mpe.mpg.de

Citation:
Paschmann, G., Sonnerup, B. U. Ö., Haaland, S. E., Phan, T.-D., & Denton, R. E. (2020). Comparison of quality measures for Walén relation. *Journal of Geophysical Research: Space Physics*, *125*, e2020JA028044. https://doi.org/10.1029/2020JA028044

Received 29 MAR 2020
Accepted 11 MAY 2020
Accepted article online 15 MAY 2020

©2020. The Authors.
This is an open access article under the terms of the Creative Commons Attribution-NonCommercial-NoDerivs License, which permits use and distribution in any medium, provided the original work is properly cited, the use is non-commercial and no modifications or adaptations are made.

Abstract The standard method for identifying magnetohydrodynamic rotational discontinuities in spacecraft data has been to examine how well the Walén relation is satisfied. In this paper, we apply two different versions of the Walén test to a database of nearly 1,000 dayside magnetopause crossings by the Magnetospheric Multi-Scale spacecraft, with the objective of comparing their performance. The first approach is to evaluate the Walén relation as a jump condition, by determining the level of agreement between the change in plasma velocity across a discontinuity with the corresponding change in the Alfvén velocity. For this purpose, we use a recently developed quality index, Q, for which $Q = \pm 1$ indicates perfect agreement. As was the case for a previously used quality index, ΔV^*, this new index employs data from two carefully chosen measurement times, located on opposite sides of the discontinuity. The second approach is to check the level of Alfvénicity of the flow for all measurements between those two points. Here, the quality index used is W_{sl}, the slope of the regression line in a scatter plot of plasma velocity components (after transformation into the deHoffmann-Teller frame) versus the corresponding Alfvén velocity components, with $W_{sl} = \pm 1$ indicating perfect agreement. For the two indices to give comparable numbers of rotational discontinuity candidates, a substantially higher threshold value is needed for $|Q|$ than for $|W_{sl}|$. Even so, the events selected by the two methods are not identical. We also identify statistical relationships between W_{sl} and its associated correlation coefficient, W_{cc}, as well as between W_{sl} and Q and between W_{sl} and ΔV^*.

1. Introduction

The classification of magnetopause and other current sheets as tangential discontinuities (TDs) or rotational discontinuities (RDs) has commonly been achieved by checking how well the plasma flow and magnetic field data satisfy the so-called Walén relation (Walén, 1944). This relation holds for RDs, which are a type of large-amplitude Alfvén waves, but usually not for TDs. The first prediction that RDs, along with slow mode structures, in the form of expansion fans, could be a common part of the reconnection geometry at the magnetopause was made by Levy et al. (1964), although RDs not necessarily related to reconnection may also occur, for example, in the solar wind (e.g., Neugebauer, 2006).

An RD has a magnetic field component and an associated flow component normal to the layer, providing magnetic coupling and flow across it, while such coupling/flow is absent across TDs. These normal components are usually small, at least at the magnetopause, so that their presence is difficult to establish with confidence from measured data. For this reason, they usually do not provide a simple and reliable way to distinguish between the two types of current layer. Instead, the distinction has been based on how well the Walén relation is satisfied, which we refer to as the Walén test.

According to the Walén relation, the plasma flow immediately upstream and downstream of an ideal RD is Alfvénic, when viewed in a comoving frame of reference (the deHoffmann-Teller [HT] frame), such that the flow, as seen in this frame, is either field aligned or anti-field aligned. The implication is that the small flow component perpendicular to the current layer is also Alfvénic on the two sides and correspondingly aligned or anti-aligned. The presence of a plasma flow across RDs is what allows us to use the terms "upstream" and "downstream" to identify its two sides; at the magnetopause, the upstream side is usually also the magnetosheath side, while the downstream side marks the end of the RD and the beginning of slow mode structures in the form of expansion fans and/or shocks and may include a reversal to outward directed flow. In its simplest magnetohydrodynamic (MHD) form, the Walén relation expresses the balance between inertia forces and magnetic stresses in RDs.

Two basic ways exist to quantify the level of agreement of measured data with the Walén relation. In the first version (Hudson, 1970), the relation is expressed as the equality of the jump, $\Delta \boldsymbol{V}$, in the plasma velocity and the jump, $\Delta \boldsymbol{V}_{\mathrm{A}}$, in Alfvén velocity, between two characteristic times, upstream and downstream of the RD. For the jump version of the Walén relation, only velocity, mass density, magnetic field, and pressure anisotropy measurements at those two times are needed. This approach allows for the study of rapidly moving layers or very thin layers.

Alternatively, the Walén relation can be cast as a continuous comparison between $\boldsymbol{V}' = (\boldsymbol{V} - \boldsymbol{V}_{HT})$, the plasma velocity evaluated in the HT frame, and $\boldsymbol{V}_{\mathrm{A}}$, for all plasma and magnetic field samples taken between the two characteristic times. The level of agreement with the Walén relation can then be visually evaluated in a component-by-component scatterplot of $\boldsymbol{V}'$ versus $\boldsymbol{V}_{\mathrm{A}}$. The overall level of agreement with the Walén relation is quantified via the regression line slope, W_{sl}, and the associated correlation coefficient, W_{cc}, the ideal values being $W_{sl} = \pm 1$ and $W_{cc} = \pm 1$. This continuous version is based on two additional assumptions, namely, that a high quality HT frame exists, which is not always the case, and that the flow remains Alfvénic throughout the RD structure, which is actually not required for an RD and is not always the case, especially for ion-scale layers. The jump version does not require these assumptions. We also note that a more general formulation of the jump version exists, in which MHD slow-mode structures are included (e.g., Eriksson et al., 2004). We have not used this version because such structures can corrupt the results for W_{sl} and W_{cc}.

In this paper, we compare the quality measures resulting from the jump version and the continuous version of the Walén test and their resulting statistics concerning the occurrence frequency of RDs at the magnetopause. Specifically, we examine the relationship between a recently proposed single quality measure, Q, for the Walén test based on the jump condition (Sonnerup et al., 2018) and the Walén-slope, W_{sl}, obtained from the continuous method. We also compare W_{sl} with an earlier quality measure, ΔV^{*}. Using the jump version in a step-by-step manner through the data intervals selected for analysis, as was done by Chao et al. (2014) for solar wind data, is an interesting further possibility, not pursued here.

For the determination of the quality measures, we used magnetic field data provided by the Fluxgate Magnetometer (FGM), described in Russell et al. (2016), and the ion and electron plasma data provided by the Fast Plasma Investigation (FPI), described in Pollock et al. (2016), all part of the Magnetospheric Multi Scale (MMS) mission and stored in a recently developed magnetopause data base (Paschmann et al., 2018).

2. Walén Relation as a Jump Condition

When expressed as a jump relation, the Walén relation can be tested directly in the spacecraft frame and has the simple form

$$\Delta \boldsymbol{V} = \pm \Delta \boldsymbol{V}_{\mathrm{A}}, \tag{1}$$

where the symbol Δ refers to changes in the plasma velocity, $\boldsymbol{V}$, and Alfvén velocity, $\boldsymbol{V}_{\mathrm{A}}$, between an upstream and a downstream station. At the magnetopause, "upstream" refers to a location in the magnetosheath adjacent to magnetopause current layer, and "downstream" refers to a station on the magnetospheric side, which we have taken as the time of maximum change in flow velocity vector, $|\Delta \boldsymbol{V}|$, following Phan et al. (1996, 2013). It is noted that this choice of the downstream state, while operationally simple, may in some cases corrupt the results by including some of the slow-mode behavior on the magnetospheric side. The $\pm$ sign in the equation refers to the fact that the Δ changes can be either parallel (+) or anti parallel (−).

For an ideal RD, the vector jumps $\Delta \boldsymbol{V}$ and $\Delta \boldsymbol{V}_{\mathrm{A}}$ should have equal magnitude, and the angle Θ between them should be either 0° or 180°, for crossings north and south of a presumed reconnection site, respectively. Note that the Alfvén velocity includes the effect of pressure anisotropy, $\boldsymbol{V}_{\mathrm{A}} = \boldsymbol{B}\sqrt{(1-\alpha)/\mu_0 \rho}$, with $\alpha = (p_{\parallel} - p_{\perp})\mu_0 / B^2$. It has been calculated from the FPI ion density assuming a 4% concentration of He^{++} particles, to represent the average solar wind composition.

2.1. Ratio R and Angle Θ of Velocity Jump Vectors

A complete evaluation of the level of agreement with the Walén relation requires two scalar quality measures, such as the magnitude ratio $R = |\Delta \boldsymbol{V}|/|\Delta \boldsymbol{V}_{\mathrm{A}}|$ and the angle, Θ, between $\Delta \boldsymbol{V}$ and $\Delta \boldsymbol{V}_{\mathrm{A}}$, as has been done

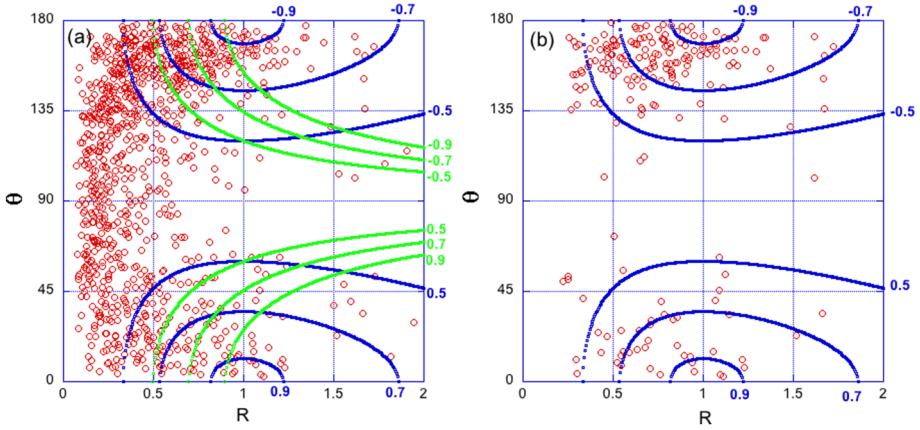

Figure 1. Scatter plots of the angle, Θ, between $\Delta \boldsymbol{V}$ and $\Delta \boldsymbol{V}_A$ versus the ratio $R = |\Delta \boldsymbol{V}|/|\Delta \boldsymbol{V}_A|$. (a) For the 994 magnetopause crossings by MMS 2 that meet the conditions listed in section 2.1 ($|Y_{GSE}|<10R_E$, magnetic shear $> 45°$, flow speed $V_{max} \geq V_{up}$). (b) For the 207 crossings that meet the additional condition that $|\Delta \boldsymbol{V}_L| > 250$ km/s. Blue curves represent locations of constant Walén quality measure, $|Q|$, for values 0.5, 0.7, and 0.9. Green curves in (a) are locations of constant quality measure ΔV^*, for those same values. The measures Q and ΔV^* are discussed in section 2.2.

in a number of magnetopause studies (e.g., Phan et al., 1996, 2013; Paschmann et al., 1986, 2018; Retinò et al., 2005; Sonnerup et al., 1981; Trenchi et al., 2008).

Figure 1a shows a scatter plot of Θ versus R, for the 994 magnetopause crossings, obtained by querying the MMS 2 database (Paschmann et al., 2018) for magnetopause crossings that were complete, located within GSE $|Y| \leq 10R_E$, had magnetic shear angles ≥45°, and had a bulk speed at the time of maximum $|\Delta \boldsymbol{V}|$ that was larger than the bulk speed V_{up} at the upstream side. We note that the above bulk speed requirement, which was also used by Paschmann et al. (2018) and Sonnerup et al. (2018), excludes a limited number of potential reconnection events in which the magnetic tension was such as to reduce the plasma speed in the exhaust jet.

Figure 1b is the same scatter plot, but now for the subset of crossings where there was pronounced jetting, identified by requiring that the magnitude of the L component of the velocity difference, $|\Delta \boldsymbol{V}_L|$, exceeded 250 km/s (the L axis is the maximum magnetic variance direction, used for no other purpose in the present paper). The predominance of events at large Θ angles in both plots indicates that a majority of crossings occurred southward of a presumed reconnection X line.

Of the 994 events shown in Figure 1a, a total of 252 (= 25.3%) meet the commonly used acceptance criterion, $R > 0.5$, and $\Theta \leq 30°$ or $\Theta \geq 150°$. For the 207 jetting events shown in Figure 1b, the number of events in the same ranges of R and Θ is 121, which makes the percentage increase to 58.8%. These numbers are in the same range as those reported for an earlier version of the database (Paschmann et al., 2018) and demonstrate that substantial plasma jetting on its own is a strong indicator for reconnection related RDs.

A notable feature along the left edge of both plots is the absence of events having a range of very small R values. The reason for the narrow gap in the left plot remains unclear. It is not caused by the limitation to shear angles ≥45°. The much wider gap in the right plot is caused by the added requirement of substantial jetting.

We have used FPI ion densities, bulk velocities, and pressures in these and the subsequent analyses, all of which would be affected by the presence of significant numbers of minor ions, especially O^+ of ionospheric origin, undifferentiated from other ions in the FPI measurements, or cold ions hidden to FPI altogether. Provided the O^+ and H^+ ions maintain nearly the same velocity component along the magnetic field, the main effect is an increase of the true mass density, which leads to a lowering of the Alfvén speed. For example, a value of 2% O^+ in a magnetopause RD would decrease that speed by about 15%, thereby increasing the Walén slope by 15%. While minor ion species are measured by the Hot Plasma Composition Analyzer (HPCA) instrument (Young et al., 2016), its 10-s cadence hampers its quantitative use in the database and

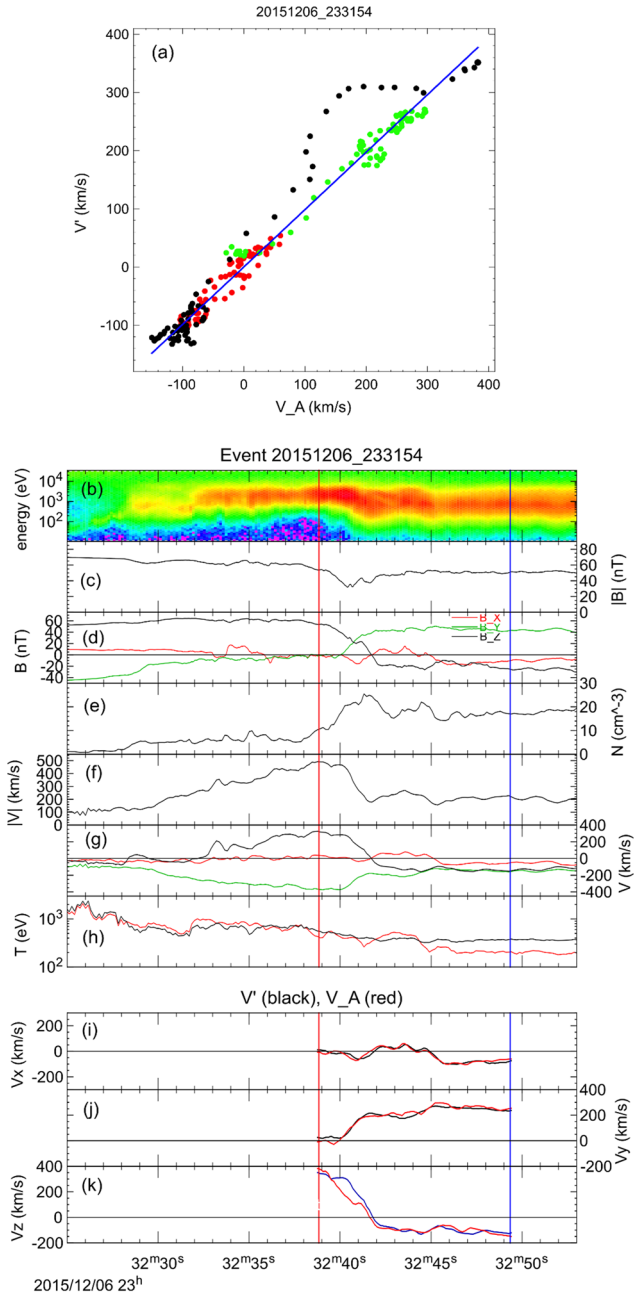

Figure 2. Outbound MMS 2 magnetopause crossing on 6 December 2015, 23:32 25 to 23:32 53 UT, at GSE location (8.4, −4.0, −0.54) R_E. (a) Scatter plot of the GSE components of $\boldsymbol{V}' = (\boldsymbol{V}-\boldsymbol{V}_{HT})$ versus the corresponding components of $\boldsymbol{V}_A$, with x, y, and z in red, green, and black, for the shorter RD data interval between the red and blue vertical lines in the time series plots below. Blue line is the regression line, with slope $W_{sl} = 0.987$ and correlation coefficient $W_{cc} = 0.981$. (b–h) Time series plots of plasma and magnetic field data (see text) for the full crossing. (i–k) GSE x, y, and z components of $\boldsymbol{V}'$ (black) together with the corresponding components of $\boldsymbol{V}_A$ (red) for the RD interval.

limits the ability to include short-duration crossings. For these reasons, we have included a standard amount of 4% He^{++} from the solar wind, rather than the actual HPCA values. And we have accommodated the possible presence of O^+ and/or ions hidden to FPI simply by using RD acceptance threshold values that are substantially less than unity.

2.2. Single Scalar Measures ΔV^* and Q

Since Equation 1 involves changes in both magnitude and direction of the vectors $\Delta\boldsymbol{V}$ and $\Delta\boldsymbol{V}_A$, it can be difficult to decide on the relative importance of those two measures. While two parameters are needed for a full characterization, a single quality measure is preferable, particularly for statistical studies. Paschmann et al. (1986) introduced the simple measure

$$\Delta V^* = R\cos\Theta, \tag{2}$$

which Phan et al. (1996) applied in the study already mentioned above and also to select RDs suitable for studies of electron and ion heating by reconnection (Phan et al., 2013, 2014).

A new single quality measure, Q, was proposed recently by Sonnerup et al. (2018), who applied it to the set of MMS 1 magnetopause crossings already studied by Paschmann et al. (2018) and compared the results to those for ΔV^*. The new index is defined as

$$Q^{\pm} = \pm\left(1 - \frac{|\Delta\boldsymbol{V} \mp \Delta\boldsymbol{V}_A|}{|\Delta\boldsymbol{V}|+|\Delta\boldsymbol{V}_A|}\right), \tag{3}$$

where the upper signs are for $\cos(\Theta) \geq 0$. In the present paper, we will refer to this index simply as Q. Its range is limited to $[-1,+1]$, while the earlier ΔV^* did not have such limits.

To illustrate how Q and ΔV^* are related to the two quality measures R and Θ, Figure 1 shows curves of constant Q (blue) and of constant ΔV^* (green) for sample values of the constants, as already discussed in Sonnerup et al. (2018). These curves illustrate how a chosen threshold for $|Q|$ limits the number of acceptable RD candidates to be located in a confined region surrounding, either the ideal value pair $R = 1$ and $\Theta = 0°$ for perfectly field aligned flow, or the value pair $R = 1$ and $\Theta = 180°$ for perfectly anti field aligned flow.

Figure 1 also shows that the green curves of constant ΔV^* extend to large R values. Specifying a lower acceptance value, or even an acceptance range, for $|\Delta V^*|$ can lead to the acceptance, not only of events that are close to perfect agreement with the Walén relation but also of some outlying events, far removed from perfect agreement. The figure makes clear that curves of constant ΔV^* do not confine events judged acceptable to be located near the two points of perfect agreement in the R,Θ plane. Note also that ΔV^* can have values around ±1 even for large R values, provided the angle Θ approaches 90°. In this regard, Q is superior to ΔV^*.

A notable feature of the family of blue curves is that the curve for $Q = 0$ (not shown in the figure) is simply the vertical axis (at $R = 0$). For a range of small $|Q|$ values (viz., $0<|Q|<0.293$; Sonnerup et al., 2018), each pair of blue curves actually intersects the horizontal axis located at $\Theta = 90°$. Beyond that range, the blue curves no longer reach $\Theta = 90°$ and take on

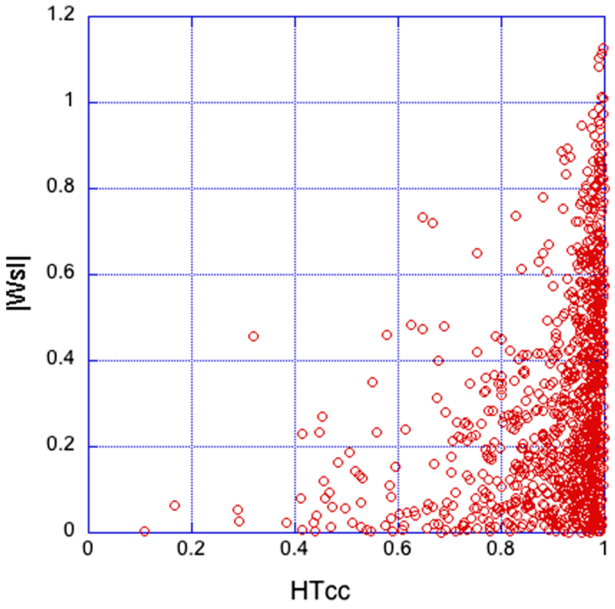

Figure 3. Scatter plot of the Walén slope, $|W_{sl}|$, versus the quality measure of the HT-frame determination, HT_{cc}, for the 994 crossings of Figure 1.

the looped shapes shown in the figure. In combination with the previously noted absence of events having very small R values, this behavior leads to the absence in the database of events having a range of sufficiently small $|Q|$ values, a result we will return to.

The behavior of the green curves for $\Delta V^* = R\cos\Theta$ in the figure is different. As $|\Delta V^*|$ decreases, they retain the basic shapes shown in the figure and approach the line $\Theta = 90°$ only as R becomes increasingly large. The green curve for $|\Delta V^*| = 0$ would consist of the vertical axis (at $R = 0$) and the horizontal axis (at $\Theta = 90°$). The result is that, in contrast to the absence of events having small $|Q|$ values, there are many events for which $|\Delta V^*|$ is small.

The relationship between ΔV^* and Q has complicated details, described by Sonnerup et al. (2018). As shown in their Figure 3, these two quality measures on average increase and decrease together but in a manner constrained by the existence of certain forbidden regions in the (Q, ΔV^*) plane. The data points for individual events have a tendency to be concentrated near the boundaries of these regions. In the allowed regions of the plane, the spread of ΔV^* values for a chosen value of Q can be large but decreases with increasing $|Q|$, an effect that can also be seen in our Figure 1.

3. Continuous Walén Relation in the deHoffmann-Teller Frame

When expressed in the HT frame (Khrabrov & Sonnerup, 1998; Sonnerup et al., 1987), the formula for the continuous Walén-relation is simply

$$\boldsymbol{V}' = \pm \boldsymbol{V}_{\mathrm{A}}, \tag{4}$$

where $\boldsymbol{V}' = (\boldsymbol{V} - \boldsymbol{V}_{\mathrm{HT}})$ is the plasma velocity evaluated in the HT frame. The term "continuous" is used here to indicate that all plasma velocity and Alfvén velocity measurements in the time interval between (and at) the chosen upstream and downstream times are used. However, depending on purpose, only portions of that interval may sometimes be preferred. (The extreme lower limit, to be employed in Appendix B, is to use only the upstream and downstream vectors.)

In the HT frame, testing of the Walén relation can consist of generating a single component-by-component scatter plot of the measured plasma velocity components, transformed into the HT frame, and the corresponding calculated Alfvén velocity components for the set of data points in the time interval given by the upstream and downstream reference times. Such a plot is shown in Figure 2a for a sample MMS magnetopause crossing. The quality of the agreement with the Walén relation is measured by the regression line slope, W_{sl}, and the associated correlation coefficient, W_{cc}. Here W_{sl} provides a measure similar to (but not identical to) the average of the ratios $r = |\boldsymbol{V}'|/|\boldsymbol{V}_{\mathrm{A}}|$, while W_{cc} is a measure of the average cosine of the angular deviation, θ, between individual vectors in each pair $\boldsymbol{V}'$ and $\boldsymbol{V}_{\mathrm{A}}$ (Paschmann et al., 2013). The quality values for this event, $W_{sl} = 0.987$ and $W_{cc} = 0.981$, along with $Q = 0.950$ and $\Delta V^* = 0.948$, all indicate that the event is an encounter with a nearly perfect RD, located north of a presumed reconnection site. Note however that a subset of the black (GSE z component) points in the scatter plot shows substantial localized deviation from the regression line.

A scatter plot destroys the time order of the measurements. It is therefore useful to compare the time series of the components of $\boldsymbol{V}'$ with those of $\boldsymbol{V}_{\mathrm{A}}$, as shown in Figures 2i–2k. To provide context, key plasma quantities for the full outbound magnetopause crossing are also shown: (Figure 2b) ion energy spectrogram; (Figure 2c) magnetic field magnitude and (Figure 2d) GSE components; (Figure 2e) number density; (Figure 2f) bulk velocity magnitude and (Figure 2g) GSE components; and (Figure 2h) parallel (red) and perpendicular (black) temperatures. The blue and red vertical lines in the figure mark the upstream and downstream reference times, respectively, with the latter taken as the time of maximum $|\Delta \boldsymbol{V}|$, as already noted.

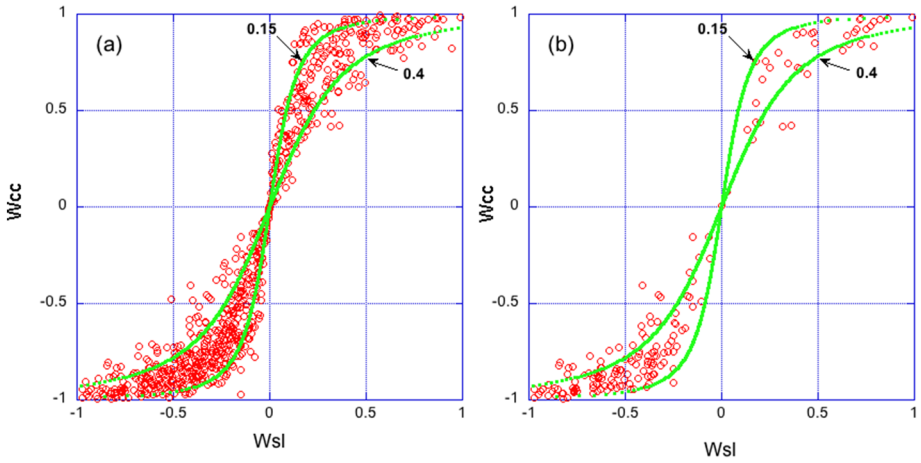

Figure 4. Scatter plot of W_{cc} versus W_{sl}, for the 791 (a) and 180 (b) crossings, the subsets of the crossings in Figure 1 that have HT-frames with $HT_{cc} > 0.85$. In both panels, theoretical curves for W_{cc} versus W_{sl} have been superimposed (in green) for two values (0.15 and 0.4) of the constant k in the underlying equation (see text and Appendix A). A few events having $|W_{sl}| > 1$ are included in the number counts but not shown.

Figure 2 illustrates how the temporary deviations between the black and red curves in panels (i)–(k) are mainly manifested as a substantial localized deviation of Vz' (black points) from the regression line in panel (a). This behavior indicates locally super-Alfvénic flow in a portion of the RD structure, but Alfvénic behavior at both the upstream and the downstream reference times, possibly as a consequence of the RD being very thin. Detailed analysis of this feature is beyond the scope of the present paper. This event illustrates not only that deviations from Alfvénic behavior can occur in the interior of what appears to be an almost perfect RD but also that the observed substantial local deviations of the z component from the regression line cause little degradation of the quality measures W_{sl} and W_{cc}.

The procedure for determining the HT frame consists of finding the transformation velocity, $\boldsymbol{V}_{\mathrm{HT}}$, from the spacecraft frame to the HT frame that minimizes the residual ion convection electric field in the least squares sense, with the quality of the HT frame velocity measured by the correlation coefficient, HT_{cc} (Khrabrov & Sonnerup, 1998; Sonnerup et al., 1987). While we use a good HT frame satisfying $HT_{cc} > 0.85$ as a prerequisite for applying the continuous Walén relation (e.g., $HT_{cc} = 0.990$ in Figure 2), this requirement by no means guarantees that the Walén relation is satisfied. This fact is demonstrated by Figure 3, which shows that the Walén-slope magnitude, $|W_{sl}|$, can assume the full range of values between 0 and slightly above 1, when HT_{cc} is large.

Figures 4a and 4b show scatter plots of W_{cc} versus W_{sl} for 791 and 180 events, the subsets of the crossings in Figures 1a and 1b, respectively, that meet the requirement $HT_{cc} > 0.85$. In Appendix A, we show that W_{cc} and W_{sl} are statistically related by the function $W_{sl} = k \cdot W_{cc}/\sqrt{1 - W_{cc}^2}$ (or, equivalently, its inverse: $W_{cc} = W_{sl}/\sqrt{k^2 + W_{sl}^2}$), where the constant k is proportional to the average fluctuation level around the regression line of the three $\boldsymbol{V}'$ components in the Walén scatter plot. In this plot, curves of that function for $k = 0.15$ and for $k = 0.4$ are superimposed on the data, with the values chosen to encompass most of the events.

As shown in Appendix A of the article by Paschmann et al. (2013), $\theta_{cc} = \cos^{-1} W_{cc}$, where W_{cc} is the correlation coefficient, is a measure of the average angular deviation, θ, between $\boldsymbol{V}'$ and $\boldsymbol{V}_{\mathrm{A}}$. We emphasize that the pair $r = |\boldsymbol{V}'|/|\boldsymbol{V}_{\mathrm{A}}|$ and θ, the magnitude ratio and the angle between individual vector pairs, $\boldsymbol{V}'$ and $\boldsymbol{V}_{\mathrm{A}}$ in an event, is not the same as the pair, R and Θ, which refers to the vectors $\Delta\boldsymbol{V}$ and $\Delta\boldsymbol{V}_{\mathrm{A}}$. For any chosen event, there is a large number of the former pairs but only one of the latter.

Figure 5 shows scatter plots of θ_{cc} versus W_{sl} for the same events as were used in Figure 4, with the function $W_{sl} = k \cot\theta_{cc}$, which follows from Equation A6 , superimposed. The figure shows that for events with $|W_{sl}| > 0.5$, the angle θ_{cc} is mostly <30° or > 150°. In terms of numbers we find that of the 791 events in the left plot, 151 (= 19.1%) have $|W_{sl}| > 0.5$ and θ_{cc} within 30° of either 0° or 180°. In the subset of 180 events in the right plot, 70 (= 38.9%) are located in the same ranges of W_{sl} and θ_{cc}.

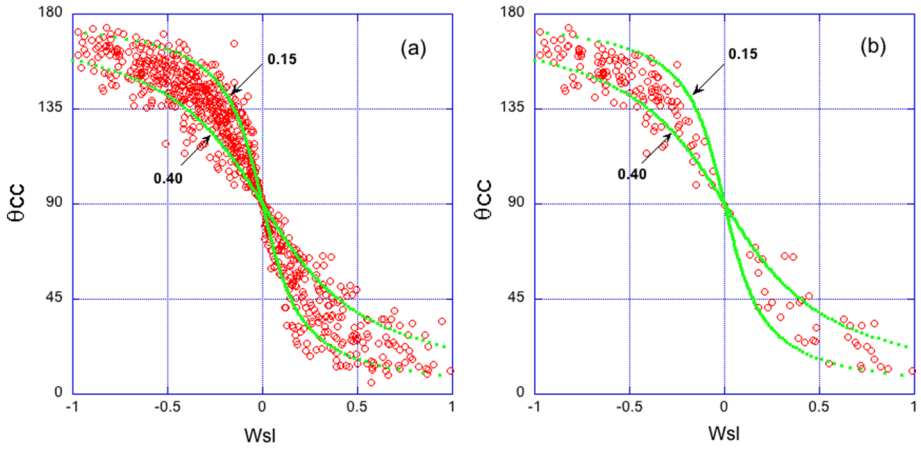

Figure 5. Scatter plots of $\theta_{cc} = \cos^{-1} W_{cc}$ versus W_{sl}, for the same sets of crossings as in Figure 4, with theoretical curves (see text and Appendix A) superimposed for two values (0.15 and 0.4) of the constant.

Appendix A in the paper by Paschmann et al. (2013) also shows that the angle $\theta_{cc} = \cos^{-1} W_{cc}$ is actually not the exact average angle between $\boldsymbol{V}'$ and $\boldsymbol{V}_{\mathrm{A}}$. The exact angle is $\theta'_{cc} = \cos^{-1} W_{cc'}$, with $W_{cc'}$ being the modified Pearson correlation coefficient, in which the averages have not been subtracted. The $W_{cc'}$ values are not available in our database, but Figure A1 in Paschmann et al. (2013) indicates that the two angles, θ and θ', are mostly very close.

The Walén relation in the HT frame has been applied previously to a substantial number of magnetopause crossings (Chou & Hau, 2012; Haaland et al., 2014, 2019; Hasegawa et al., 2010; Nykyri et al., 2006; Phan et al., 2004; Paschmann et al., 2005; Sonnerup et al., 1990), and to discontinuities in the solar wind (Gosling et al., 2005; Paschmann et al., 2013). In many of these studies, events with a well-defined HT frame and Walén regression line slopes exceeding some level were classified as RDs, without considering the role of the correlation coefficient W_{cc} as a measure of the average angle θ between $\vec{V}'$ and $\vec{V}_{\mathrm{A}}$. As Figure 5, shows, selecting RD candidates by just requiring $W_{sl} > 0.5$, say, also limits the corresponding θ deviation from the ideal value of 0° or 180° to be less than about 30° for most of the events. As a consequence, relying solely on W_{sl} as a quality measure may often be permissible.

4. Relationships of Q and ΔV^* to W_{sl}

As we have already noted, there is an important difference between tests of the jump version of the Walén relation in the spacecraft frame and the continuous version in the HT frame: In the version we use, the former is based solely on data at two selected times, while the latter also includes a potentially large number of field/plasma samples in the entire interval between those two times. The first comparison of the statistics obtained with the jump version and the continuous version can be found in a recent paper by Haaland et al. (2020). Their figure 4 presents histograms of $|Q|$ and $|W_{sl}|$ for a large number of magnetopause crossings by MMS 2, with emphasis on crossings at the flanks, which are not included in the present study. Those histograms exhibit a much larger fraction of events having $|Q| > 0.5$ than of events having $|W_{sl}| > 0.5$, a result that has served to motivate our present study.

4.1. Q Versus W_{sl}

Figure 6 shows scatter plots of Q versus W_{sl} for the same 791 and 180 crossings with $HT_{cc} > 0.85$ used for Figure 4. It shows that most of the points are found on the side of the diagonal, shown green, where $|Q| > |W_{sl}|$. In other words, there are many more points with $|Q| > 0.5$ than with $|W_{sl}| > 0.5$. In numbers, 298 of the 791 points (43%) in the left plot have $|Q| > 0.5$, but only 136 (20%) have $|W_{sl}| > 0.5$. For the 180 points in the right plot, both percentages increase, as expected for cases with pronounced jetting, but the percentage for $|W_{sl}| > 0.5$ remains much less than the percentage for $|Q| > 0.5$ (90% have $|Q| > 0.5$, while only 51% have $|W_{sl}| > 0.5$).

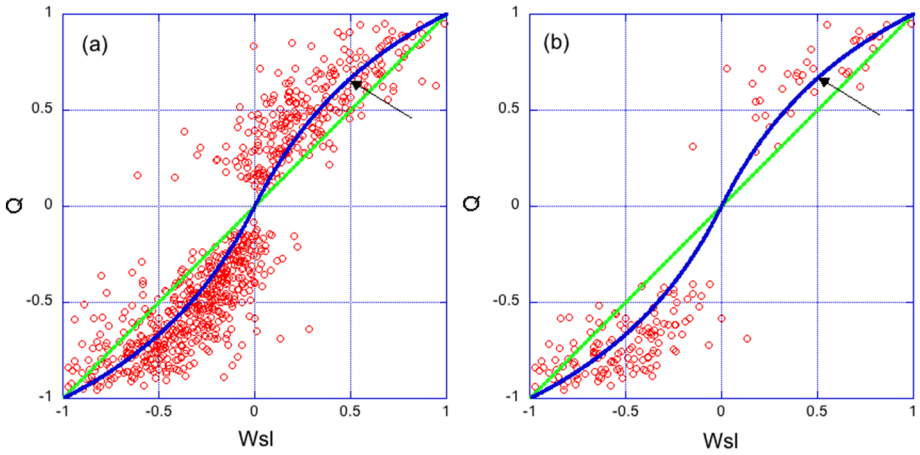

Figure 6. Scatter plots of Q versus W_{sl}, in panel (a) for all 791 magnetopause crossings having $HT_{cc} > 0.85$ in addition to the criteria used for the events of Figure 1a; (b) for those 180 that also have strong jetting. A blue curve shows the function $Q = 2W_{sl}/(1+|W_{sl}|)$, valid for $\theta = 0°$ or 180°, in combination with the assumption of a perfect HT frame ($HT_{cc} = \pm 1$). Black arrows mark the point on the blue curve where $\theta = 0$ and $W_{sl} = 0.5$, for which $Q = 2/3$, with geometry discussed in Appendix B.

As expected from the discussion of Figure 1, the figure also shows that no events are located near $Q = 0$.

That the asymmetric distribution of points around the green diagonal line can be expected is illustrated by the blue curve in the figure. This theoretical curve is based on an expression for Q in terms of the ratio R and the angle Θ between the two Δ vectors in Equation 1, together with the intrinsic assumption that a perfect HT frame of reference exists. For the top half of the diagram in the figure, this equation is (see equation A.2 in the paper by Sonnerup et al. (2018), in which the letters r and θ were used instead of R and Θ):

$$Q = 1 - \frac{\sqrt{R^2 + 1 - 2R\cos\Theta}}{R+1}, \tag{5}$$

where $R = |\Delta \boldsymbol{V}|/|\Delta \boldsymbol{V}_A|$ and $\cos\Theta = (\Delta \boldsymbol{V} \cdot \Delta \boldsymbol{V}_A)/(|\Delta \boldsymbol{V}||\Delta \boldsymbol{V}_A|)$. For $\Theta = \theta = 0°$, we can interpret the Walén slope simply as $W_{sl} = R = r$. In Figure 6, Equation 5 then reduces to $Q = 2\,W_{sl}/(1+W_{sl})$; it is shown by the blue curve. The point on this curve where $W_{sl} = 0.5$ and $Q = 2/3$ is identified by a black arrow. The corresponding vector geometry is shown in Figure B1.

For $\Theta \neq 0$, we no longer have $W_{sl} = R$. The situation is now more complicated and depends on additional geometrical features such as the magnetic shear angle, as discussed in Appendix B. We have no simple explanation for the asymmetric spread of event points around the blue curve.

Figure 6 makes clear that to get comparable statistics, one cannot use the same lower cutoff values for $|Q|$ as for $|W_{sl}|$. In case of the 791 events, the threshold for $|Q|$ would have to be increased to 0.71 to lower the resulting number of events to the number we have for $|W_{sl}| > 0.5$ (196), and similarly for the case of the 180 jetting events, where the threshold for $|Q|$ would have to be increased to 0.73 to get equal numbers of events (92). We note that making the number of events come out equal does not mean that all the selected cases are the same. For example, of the 92 events that result from requiring either $|W_{sl}| > 0.5$ or $|Q| > 0.73$, only 69 of the events are in both sets.

4.2. ΔV^* Versus W_{sl}

For a comparison with Figure 6, Figure 7 shows, on the left, the scatter plot of ΔV^* versus W_{sl} for the same set of 791 crossings. It shows an overall correlation between the two quality measures, with linear regression line slope of 1.24 and correlation coefficient of 0.79, and therefore an excess of events with $\Delta V^* > 0.5$ over those with $W_{sl} > 0.5$. In this plot there are many event locations around $\Delta V^* = 0$, which was already explained in the discussion of Figure 1. In the plot on the right for the 180 events with strong jetting, there is an empty band around $\Delta V^* = 0$, resulting from the absence of points having small values of $|\Delta V^*|$ in Figure 1b.

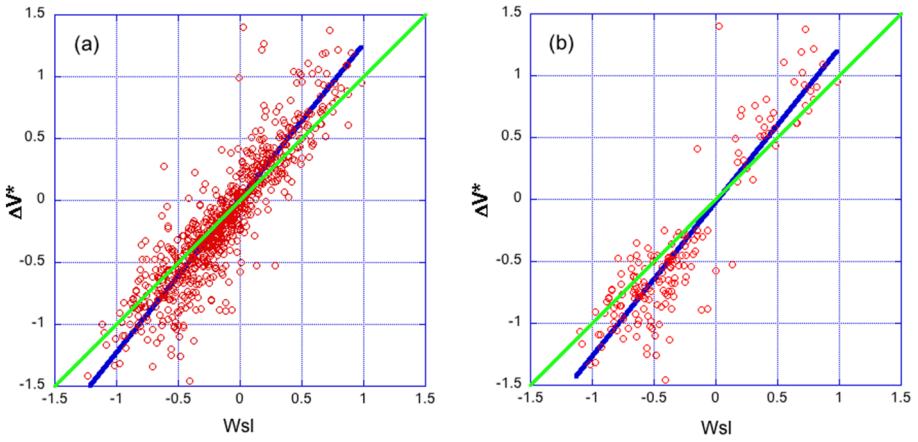

Figure 7. Scatter plots of ΔV^* versus W_{sl}; (a) for the 791 and (b) for the 180 crossings, as in Figure 6. The green lines are diagonals, and the blue lines are regression lines, with slopes of 1.24 in both plots and correlation coefficients of 0.79 in (a) and 0.90 in (b).

Overall, the plot indicates that the earlier use of ΔV^* as a single scalar quality measure had considerable merit, most notably its simplicity. As noted already for Q, to get comparable statistics, one cannot use the same threshold for ΔV^* as for $|W_{sl}|$. In case of the 791 events, the threshold for $|\Delta V^*|$ would have to be increased to 0.64 to get about the same number of events as for $|W_{sl}| > 0.5$, and similarly for the case of the 180 jetting events, where the threshold for $|\Delta V^*|$ would have to be increased to 0.68 to get equal numbers of events.

5. Method Comparison

Figure 8 shows a comparison between various measures for the Walén-relation tests. The ratio $R = |\Delta \boldsymbol{V}|/|\Delta \boldsymbol{V}_A|$ and the angle Θ between $\Delta \boldsymbol{V}$ and $\Delta \boldsymbol{V}_A$ are the most complete indicators of the agreement of an event with the jump version of the Walén relation. The red-colored and light blue-colored data points in the figure identify events with $|W_{sl}|<0.5$ (red) and $|W_{sl}| > 0.5$ (blue). It is seen that red and blue cases are intermixed but with blue events better concentrated around the two points of perfect agreement with the Walén relation (at $R = 1$ and either $\Theta = 0°$ or $\Theta = 180°$). The blue contours of constant Q illustrate how increasingly strict acceptance threshold levels for Q lead to the selection of events in regions of decreasing size surrounding

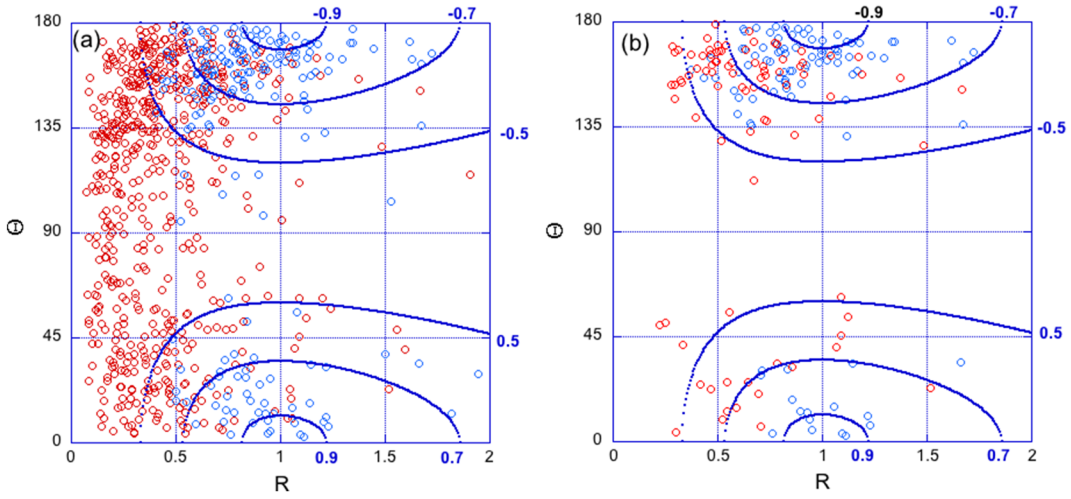

Figure 8. Scatter plots of Θ versus R, for the 791 and 180 magnetopause crossings by MMS 2, respectively, with $HT_{cc} > 0{,}85$. Events with Walén slopes $|W_{sl}|<0.5$ are shown in red, those with $|W_{sl}| > 0.5$ in light blue. Solid blue curves are as in Figure 1.

Table 1
Walén Relation Statistics

Quality measure	791 crossings[a]	180 crossings[b]
$R > 0.5$ and $\Theta<30°$[c]	180 (22.7%)	93 (51.7%)
$Q > 0.5$	416 (52.5%)	162 (90.0%)
$Q > 0.7$	202 (25.5%)	105 (58.3%)
$W_{sl} > 0.5$	196 (24.7%)	92 (51.1%)
$Q > 0.7$ and $W_{sl} > 0.5$	137 (17.3%)	77 (42.8%)

[a]MP crossings with $|Y_{GSE}|<10\,R_E$, magnetic shear $> 45°$, $HT_{cc} > 0.85$, and $V_{max}/V_{up} \geq 1$. [b]As in Note (a) but with the added requirement $|\Delta V_L| > 250$ km/s. [c]Or $> 150°$.

the two points of perfect agreement. The curves for $Q = \pm 0.5$ enclose many more red cases than blue cases; most of the latter are located inside the curves for $Q = \pm 0.7$.

As Table 1 shows, to catch a similar number of acceptable RD events, one could either use events that fall in a specified area of the (R,Θ) plane (e.g., $R > 0.5$ and Θ within 30° of either 0° or 180°), or events for which the Walén slopes are $|W_{sl}| > 0.5$, or events for which $|Q| > 0.7$. The table also shows that the numbers for $|Q| > 0.5$ are very much larger than those for $|W_{sl}| > 0.5$, indicating again that using equal numerical thresholds for W_{sl} and Q to estimate the occurrence frequency of RDs is not supported by the data.

The similarity of the conditions $|W_{sl}| > 0.5$ and $|Q| > 0.7$ is apparent in Figure 8 as well. But the figure also shows that there are quite a number of events with $|W_{sl}| > 0.5$ but $|Q|<0.7$, and similarly a number of events with $|W_{sl}|<0.5$ but $|Q| > 0.7$. This shows that the two are not equivalent, which is not surprising, given the fundamentally different nature of the test underlying the Q and W_{sl} parameters. As we said before, for a complete specification, two parameters are needed, such as R and Θ. But one can also remove the noted inconsistency between the events selected by $|W_{sl}| > 0.5$ and by $|Q| > 0.7$, by combining their respective thresholds. This reduces the number of RD candidates to 17.3% for the full set of crossings and to 42.8% for the subset of crossings with pronounced jetting, as shown in the bottom line of Table 1.

6. Summary and Discussion

The classification of magnetopause and other current sheet crossings as containing RDs has commonly been achieved by checking how well the plasma flow and magnetic field data satisfy the Walén relation. Two fundamentally different approaches exist. The first method is to select two times, one upstream and one downstream of the potential RD, and compare the jump in plasma velocity between the two times with the associated jump in Alfvén velocity. In this case, the success has typically been expressed by two measures: how close the ratio $R = |\Delta \boldsymbol{V}|/|\Delta \boldsymbol{V}_A|$ is to unity and how close the angle, Θ, between $\Delta \boldsymbol{V}$ and $\Delta \boldsymbol{V}_A$, is to either 0° or to 180° (see Figure 1). More convenient, particularly for statistical studies, is to use a single scalar quality measure, Q, which has been proposed recently (Sonnerup et al., 2018) as an improvement over a previously used measure, ΔV^*.

The second method is to use all measurements in the interval between the upstream and downstream times to obtain a continuous comparison between the plasma velocity samples (after they have been transformed into the HT frame) and the associated Alfvén velocity samples. In this case, the degree of success is expressed by two quantities, namely, the slope, W_{sl}, and correlation coefficient, W_{cc}, of the linear regression line in the scatter plot of the components of $\boldsymbol{V}'$ versus the corresponding components of $\boldsymbol{V}_A$ (see Figure 2). These two quantities are qualitative counterparts of the ratio, R, and the angle, Θ, used in the jump-relation formulation of the Walén test.

Both methods have been widely used in earlier studies, as evident from citations in the previous sections, but they have not been directly compared in detail. To overcome this dilemma, we have applied the Walén relation in these two different forms to the dayside magnetopause crossings from the MMS 2 database described by Paschmann et al. (2018) and have compared their various measures of success. The dual quality measures R and Θ, as well as the single measures Q and ΔV^*, were calculated from the plasma and magnetic field data stored in the database for the upstream (magnetosheath) reference time and for the time where the change in the plasma velocity reached its maximum. The Walén slopes, W_{sl}, and correlation coefficients, W_{cc}, are also stored in the database, having been calculated from all samples between (and including) those two times as part of the database production process. The main results of our study are as follows.

1. Either W_{sl}, Q, or ΔV^* can be used as a single Walén quality measure to identify potential RDs. Given the fundamentally different nature of the methods underlying W_{sl} on one hand, and Q and ΔV^* on the other, it is remarkable that they statistically are closely related, as shown in Figures 6 and 7. However, to obtain comparable numbers of such candidate events, the threshold value for $|Q|$ or $|\Delta V^*|$ must be substantially larger than that for $|W_{sl}|$. For the commonly used requirement $|W_{sl}| > 0.5$, the corresponding jump

versions would be approximately $|Q| > 0.71$ or $\Delta V^* > 0.64$. Even with these different thresholds, only about 70 % of the RD candidates selected by the two methods are the same. A much stricter acceptance criterion would be to require the thresholds of both W_{sl} and Q to be met, which would reduce the fraction of potential RDs to some 17% of the total pool of events (see Table 1).

2. An advantage of the jump version is that it requires minimal numerical effort and can be used with lower-resolution data. The main disadvantage is that, in the presence of substantial fluctuations, the results can be sensitive to the precise choice of the upstream and downstream times.
3. The plot of $\theta_{cc} = \cos^{-1}(W_{cc})$ versus W_{sl} (Figure 5) shows that for reasonably large $|W_{sl}|$ (> 0.5 or so), the angles θ_{cc} are mostly within 30° of either 0° or 180°, so that W_{sl} can serve as a single quality measure.
4. The advantage of the continuous method is that it is less sensitive to the choice of the upstream and downstream reference times and that it presents a more robust assessment of the overall level of Alfvénicity of the structure. The main disadvantages are that it is numerically more complicated and that the Walén relation may not hold in the interior of thin current layers. The method also depends on the quality of the HT frame determination, as measured by HT_{cc}. Note that our method to obtain the HT frame velocity is based on the ion convection electric field and that it does not take into account the possible presence of an intrinsic electric field component along the normal direction. It can be argued that the HT frame should be based on electron velocities rather than ion velocities (Scudder et al., 1999), or ideally directly on the measured electric field. For more detailed studies, the Walén scatterplot can provide helpful information, such as the presence of substructures (see, e.g., Figure 2), and/or nonlinear correlation.
5. The statistical results from the Walén relation show a continuum of behavior. They do not provide a clear distinction between RD events and TD events in the form of separate clumping of points in event scatter plots such as Figure 1. Detailed studies are required in order to establish, beyond reasonable doubt, that a potential RD candidate, identified by use of Q or W_{sl}, is actually a true RD. The Walén test is concerned with the tangential stress balance. The conservation laws for mass, normal stress, and energy, along with features of the distribution function, such as counter-streaming, can in principle be of help in confirming RD status (Phan et al., 2013). Here we have simply used the presence of substantial jetting as a reasonable additional requirement for reconnection related RDs.
6. An unresolved issue is why $|W_{sl}|$ at the magnetopause is almost always substantially less than unity, while $|W_{cc}|$ can still remain near unity (see Figure 4). This issue has been discussed by Puhl-Quinn and Scudder (2000). Another serious issue is why the mass conservation law for ideal RDs, $\rho(1-\alpha) = const$, is almost never satisfied (Blagau et al., 2015). Detailed discussion of these problems is beyond the scope of the present paper.
7. A new result of the present study is a statistical relationship between W_{sl} and W_{cc}, described by the function $W_{cc} = W_{sl}/\sqrt{k^2 + W_{sl}^2}$, where the constant k is proportional to the average fluctuation level (in the Walén scatter plot) of the three $\boldsymbol{V}'$ components around the regression line.
8. We have also established relations between the scalar quality measures. The older measure ΔV^* is shown to be statistically proportional to 1.24 W_{sl} (Figure 7). Regarding Q and W_{sl}, there is a simple prediction of the S-shaped distribution of event points in the scatter plot of Q versus W_{sl} (see blue curve in Figure 6). This relation is $Q = 2\,W_{sl}/(1 \pm W_{sl})$, which is strictly valid only for $\Theta = 0°$ or 180°.

Appendix A: Relationship Between W_{sl} and W_{cc}

In this appendix, we derive the equations plotted as the green curves in Figures 4 and 5, starting from the development given in Appendix A of Paschmann et al. (2013). For brevity, we employ the same notation used there, according to which x represents the three components of $\boldsymbol{V}_A$ on the horizontal axis of the Walén scatter plot and y the corresponding components of $\boldsymbol{V}'$ on the vertical axis. We also assume the regression line to be represented by $y = a + bx$ so that $W_{sl} = b$. And for simplicity we assume $a = 0$, along with symmetry conditions such that the averages $\langle x \rangle = \langle y \rangle = 0$. Finally, we use the notation $W_{cc} = (cc)$.

Equations A.1 and A.4 in Paschmann et al. (2013) are

$$(cc)^2 = \frac{\langle xy \rangle^2}{\langle x^2 \rangle \langle y^2 \rangle}, \tag{A1}$$

$$b^2 = \frac{\langle xy \rangle^2}{\langle x^2 \rangle^2}. \tag{A2}$$

From these expressions follows that

$$b^2 = (cc)^2 \frac{\langle y^2 \rangle}{\langle x^2 \rangle}. \tag{A3}$$

Next we describe the fluctuations of the individual points in the Walén scatter plot by the symbol δ so that

$$y = bx + \delta \tag{A4}$$

with the average $\langle \delta \rangle = 0$ so that

$$\langle y^2 \rangle = b^2 \langle x^2 \rangle + \langle \Delta^2 \rangle. \tag{A5}$$

We can now put this result into Equation A3 to obtain

$$b^2 = (cc)^2 \frac{b^2 \langle x^2 \rangle + \langle \delta^2 \rangle}{\langle x^2 \rangle}. \tag{A6}$$

Denoting the normalized standard deviation by $k = \sqrt{\langle \delta^2 \rangle / \langle x^2 \rangle}$, we can then solve for (cc) to obtain

$$(cc) = \frac{b}{\sqrt{b^2 + k^2}}. \tag{A7}$$

Returning to the notation in the main part of the paper, we have

$$W_{cc} = \frac{W_{sl}}{\sqrt{W_{sl}^2 + k^2}}. \tag{A8}$$

This expression, with $k = 0.15$ and $k = 0.4$, is represented by the green curves in Figures 4 and 5.

Appendix B: Relationship Between W_{sl} and Q

In this appendix, we discuss the theoretical relationship between the quality measure W_{sl}, which is obtained from the continuous version of the Walén relation, and the quality measure Q, which results from use of the jump version. The discussion is complicated by the fact that these two measures utilize different data sets: W_{sl} is based on all measurements during a chosen time interval, while Q is based on the data taken only at the beginning and end points of that interval.

To enable a theoretical comparison of the two versions of the Walén test, we can apply the continuous Walén test to the total of six individual components of $\boldsymbol{V}'$ and $\boldsymbol{V}_A$, based on measurements taken only at the beginning and at the end end of the interval. This is what will be done here, with the additional assumption that a perfect HT frame of reference is at hand. In this frame, the velocity vectors $\boldsymbol{V}'$ and $\boldsymbol{V}_A$ are aligned, both at the upstream and the downstream stations. These vectors therefore define a reference plane to which all vectors including the Δ vectors are confined. The vector plot shown in Figure B1 illustrates the behavior in this plane. Since the components of $\boldsymbol{V}'$ and $\boldsymbol{V}_A$ along the normal to the reference plane are zero, both upstream and downstream, two of the six data points in the Walén scatter plot, are located at the origin, leaving only four points away from the origin.

Figure B1 is a simple example where the angle $\Theta = 0$ so that the red and black Δ vectors in the figure are parallel. Since $\boldsymbol{V}'$ is also parallel to $\boldsymbol{V}_A$, both upstream and downstream, we have $\theta = 0$, both upstream (subscript 1) and downstream (subscript 2). We also have the same chosen ratio $r = 0.5$ at those two locations, because the smaller red vector triangle in the figure is similar to the larger black triangle. As a result, the ratio of the two jump vectors is $R = |\Delta \boldsymbol{V}|/|\Delta \boldsymbol{V}_A| = 0.5$ as well. In the figure, the locations of the various arrow

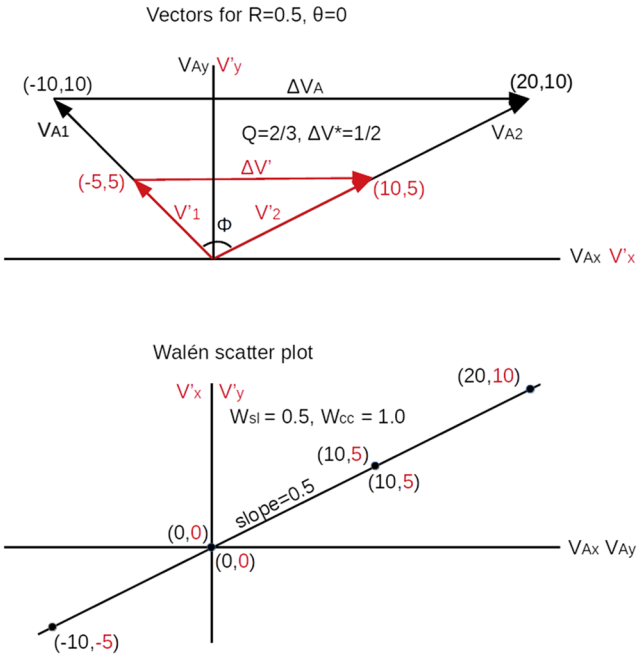

Figure B1. Example of vector geometry for which $R = 1/2$, $\Theta = 0$, and $Q = 2/3$ or, alternatively, $W_{sl} = 0.5$ and $W_{cc} = 1$, so that $\Theta_{cc} = 0$. This case has magnetic shear angle $\Phi = 108.4°$; it is marked by black arrow in Figure 6.

heads are specified (in arbitrary units). At the bottom of the figure, the corresponding Walén scatter plot is shown. It contains only six points, two of which are located at the origin (0, 0). These six points all fall exactly on a regression line with slope $W_{sl} = 0.5$ so that $W_{cc} = 1$ and therefore $\theta_{cc} = 0$. The corresponding jump-based quality value is $Q = 2/3$. This case is marked by the black arrow in Figure 6, located on the blue curve. For this case we also find $\Delta V^* = 1/2$.

When $\Theta \neq 0$, the situation is more complicated because Θ and θ, as well as R and r, are no longer the same. The results now depend on other geometrical factors such as the magnetic shear angle Φ (which is $\Phi = 108.4°$ in Figure B1) and on whether the vector $\Delta \boldsymbol{V}'$ is inclined above or below the (horizontal) vector $\Delta \boldsymbol{V}_A$ in the reference plane. For example, if the beginning and end points of the vector $\Delta \boldsymbol{V}'$ in Figure B1 are moved from (−5, 5) and (10, 5) to (−8, 8) and (4, 2), the result is that the $\Delta \boldsymbol{V}'$ vector now slopes down at an angle of $\Theta = 26.6°$. For this geometry, the corresponding coordinates in Figure 6 are $W_{sl} = 0.3412$ and $Q = 0.5630$, which would fall above the blue curve but not be far removed from it. There would now also be considerable scatter of the six data points around the regression line in the Walén scatter plot, indicating that the Walén slope has substantial uncertainty. Nevertheless, as long as the HT frame is of high quality, the blue curve seems to provide a reasonably robust prediction, even when $\Theta \neq 0$.

The conclusion is that in general there is not a one-to-one relationship between a chosen point in the (W_{sl}–Q) plane and a corresponding vector configuration. Furthermore, there is no guarantee that such a point by necessity corresponds to an actual physically realizable configuration.

Acknowledgments

G. P. was supported by a guest status at MPE, Garching. Research efforts by B. U. Ö. S. and R. E. D. were supported by NASA Grant 80NSSC19K0254 to Dartmouth College, those by S. E. H by the Norwegian Research Council under Grant 223252, and those by T.-D. P. by NASA Grants NNX17AE12G and 80NSSC18K1380. The authors are grateful to the International Space Science Institute, Bern, Switzerland, for support of ISSI Team 442, "Study of the physical processes in magnetopause and magnetosheath current sheets using a large MMS database." All MMS data are publicly available online (through the URL https://lasp.colorado.edu/mms/sdc/public/).

References

Blagau, A., Paschmann, G., Klecker, B., & Marghitu, O. (2015). Experimental test of the $\rho(1\text{-}\alpha)$ evolution for rotational discontinuities: Cluster magnetopause observations. *Annales Geophysicae*, *33*(1), 79–91. https://doi.org/10.5194/angeo-33-79-2015

Chao, J. K., Hsieh, W. C., Yang, L., & Lee, L. C. (2014). Walén test and de Hoffmann-Teller frame of interplanetary large-amplitude Alfvén waves. *Astrophysical Journal*, *786*(2), 149. https://doi.org/10.1088/0004-637X/786/2/149

Chou, Y. C., & Hau, L. N. (2012). A statistical study of magnetopause structures: Tangential versus rotational discontinuities. *Journal of Geophysical Research*, *117*, A08232. https://doi.org/10.1029/2011JA017155

Eriksson, S., Øieroset, M., Baker, D. N., Mouikis, C., Vaivads, A., Dunlop, M. W., & Balogh, A. (2004). Walén and slow-mode shock analyses in the near-Earth magnetotail in connection with a substorm onset on 27 August 2001. *Journal of Geophysical Research*, *109*, A18. https://doi.org/10.1029/2004JA010534

Gosling, J. T., Skoug, R. M., McComas, D. J., & Smith, C. W. (2005). Direct evidence for magnetic reconnection in the solar wind near 1 AU. *Journal of Geophysical Research*, *110*, 1107. https://doi.org/10.1029/2004JA010809

Haaland, S., Paschmann, G., Øieroset, M., Phan, T., Hasegawa, H., Fuselier, S. A., & Burch, J. (2020). Characteristics of the flank magnetopause: MMS results. *Journal of Geophysical Research: Space Physics*, *125*, e27623. https://doi.org/10.1002/(ISSN)2169-9402

Haaland, S., Reistad, J., Tenfjord, P., Gjerloev, J., Maes, L., DeKeyser, J., & Dorville, N. (2014). Characteristics of the flank magnetopause: Cluster observations. *Journal of Geophysical Research: Space Physics*, *119*, 9019–9037. https://doi.org/10.1002/2014JA020539

Haaland, S., Runov, A., Artemyev, A., & Angelopoulos, V. (2019). Characteristics of the flank magnetopause: THEMIS observations. *Journal of Geophysical Research: Space Physics*, *124*, 3421–3435. https://doi.org/10.1029/2019JA026459

Hasegawa, H., Wang, J., Dunlop, M. W., Pu, Z. Y., Zhang, Q. H., Lavraud, B., & Bogdanova, Y. V. (2010). Evidence for a flux transfer event generated by multiple X-line reconnection at the magnetopause. *Geophysical Reseach Letters*, *37*, 16,101. https://doi.org/10.1029/2010GL044219

Hudson, P. D. (1970). Discontinuities in an anisotropic plasma and their identification in the solar wind. *Planetary Space Science*, *18*, 1611–1622.

Khrabrov, A. V., & Sonnerup, B. U. Ö. (1998). deHoffmann-Teller analysis, *Analysis Methods for Multi-Spacecraft Data* (pp. 221). Noordwijk, The Netherlands: ESA Publications Division.

Levy, R. H., Petschek, H. E., & Siscoe, G. L. (1964). Aerodynamic aspects of the magnetopsheric flow. *AIAA Journal*, *2*, 2065.

Neugebauer, M. (2006). Comment on the abundances of rotational and tangential discontinuities in the solar wind. *Journal of Geophysical Research*, *11*, A04103. https://doi.org/10.1029/2005JA011497

Nykyri, K., Otto, A., Lavraud, B., Mouikis, C., Kistler, L. M., Balogh, A., & Rème, H. (2006). Cluster observations of reconnection due to the Kelvin-Helmholtz instability at the dawnside magnetospheric flank. *Annales Geophysicae*, *24*, 2619–2643. Retrieved from http://www.ann-geophys.net/24/2619/2006/

Paschmann, G., Haaland, S. E., Phan, T. D., Sonnerup, B. U. Ö., Burch, J. L., Torbert, R. B., & Fuselier, S. A. (2018). Large-scale survey of the structure of the dayside magnetopause by MMS. *Journal of Geophysics Research: Space Physics*, *123*, 2018–2033. https://doi.org/10.1002/2017JA025121

Paschmann, G., Haaland, S., Sonnerup, B. U. Ö., Hasegawa, H., Georgescu, E., Klecker, B., & Vaivads, A. (2005). Characteristics of the near-tail dawn magnetopause and boundary layer. *Annales Geophysiae*, *23*, 1481–1497.

Paschmann, G., Haaland, S., Sonnerup, B., & Knetter, T. (2013). Discontinuities and Alfvenic fluctuations in the solar wind. *Annales Geophysicae*, *31*, 871–887. https://doi.org/10.5194/angeo-31-871-2013

Paschmann, G., Papamastorakis, I., Baumjohann, W., Sckopke, N., Carlson, C. W., Sonnerup, B. U. Ö., & Lühr, H. (1986). The magnetopause for large magnetic shear—AMPTE/IRM observations. *Journal of Geophysical Research*, *91*, 11,099–11,115. https://doi.org/10.1029/JA091iA10p11099

Phan, T., Drake, J. F., Shay, M. A., Gosling, J. T., Paschmann, G., Eastwood, J. P., & Angelopoulos, V. (2014). Ion bulk heating in magnetic reconnection exhausts at Earth's magnetopause: Dependence on the inflow Alfvén speed and magnetic shear angle. *Geophysical Research Letters*, *41*, 7002–7010. https://doi.org/10.1002/2014GL061547

Phan, T., Dunlop, M., Paschmann, G., Klecker, B., Bosqued, J., Rème, H., & Kistler, L. (2004). Cluster observations of continuous reconnection at the magnetopause under steady interplanetary magnetic field conditions. *Annales Geophysicae*, *22*, 2355–2367. https://doi.org/10.5194/angeo-22-2355-2004

Phan, T., Paschmann, G., Gosling, J. T., Øieroset, M., Fujimoto, M., Drake, J. F., & Angelopoulos, V. (2013). The dependence of magnetic reconnection on plasma β and magnetic shear: Evidence from magnetopause observations. *Geophysical Research Letters*, *40*, 11–16. https://doi.org/10.1029/2012GL054528

Phan, T., Paschmann, G., & Sonnerup, B. U. Ö. (1996). Low-latitude dayside magnetopause and boundary layer for high magnetic shear 2. Occurrence of magnetic reconnection. *Journal of Geophysical Research*, *101*, 7817–7828. https://doi.org/10.1029/95JA03751

Pollock, C., Moore, T., Jacques, A., Burch, J., Gliese, U., Saito, Y., & Zeuch, M. (2016). Fast plasma investigation for magnetospheric multiscale. *Space Science Reviews*, *199*, 331–406. https://doi.org/10.1007/s11214-016-0245-4

Puhl-Quinn, P. A., & Scudder, J. D. (2000). Systematics of ion Walén analysis of rotational discontinuities using E/Z measurements. *Journal of Geophysical Research*, *105*, 7617–7628. https://doi.org/10.1029/1999JA000314

Retinò, A., Bavassano Cattaneo, M. B., Marcucci, M. F., Vaivads, A., André, M., Khotyaintsev, Y., & Balogh, A. (2005). Cluster multispacecraft observations at the high-latitude duskside magnetopause: Implications for continuous and component magnetic reconnection. *Annales Geophysicae*, *23*(2), 461–473. https://doi.org/10.5194/angeo-23-461-2005

Russell, C. T., Anderson, B. J., Baumjohann, W., Bromund, K. R., Dearborn, D., Fischer, D., & Richter, I. (2016). The magnetospheric multiscale magnetometers. *Space Science Reviews*, *199*, 189–256. https://doi.org/10.1007/s11214-014-0057-3

Scudder, J. D., Puhl-Quinn, P. A., Mozer, F. S., Ogilvie, K. W., & Russell, C. T. (1999). Generalized Walén tests through Alfvén waves and rotational discontinuities using electron flow velocities. *Journal of Geophysical Research*, *104*(A9), 19,817–19,834. https://doi.org/10.1029/1999JA900146

Sonnerup, B. U. Ö., Haaland, S. E., Paschmann, G., & Denton, R. E. (2018). Quality measure for the Walén relation. *Journal of Geophysical Research*, *123*, 9979–9990. https://doi.org/10.1029/2018JA025677

Sonnerup, B. U. Ö., Papamastorakis, I., Paschmann, G., & Luehr, H. (1987). Magnetopause properties from AMPTE/IRM observations of the convection electric field: Method development. *Journal of Geophysical Research*, *92*(A11), 12,137–12,159. https://doi.org/10.1029/JA092iA11p12137

Sonnerup, B. U. Ö., Papamastorakis, I., Paschmann, G., & Luehr, H. (1990). The magnetopause for large magnetic shear—Analysis of convection electric fields from AMPTE/IRM. *Journal of Geophysical Research*, *95*, 10,541–10,557. https://doi.org/10.1029/JA095iA07p10541

Sonnerup, B. U. Ö., Paschmann, G., Papamastorakis, I., Sckopke, N., Haerendel, G., Bame, S. J., & Russell, C. T. (1981). Evidence for magnetic field reconnection at the Earth's magnetopause. *Journal of Geophysical Research*, *86*, 10,049–10,067. https://doi.org/10.1029/JA086iA12p10049

Trenchi, L., Marcucci, M. F., Pallocchia, G., Consolini, G., Bavassano Cattaneo, M. B., di Lellis, A. M., & Cao, J. B. (2008). Occurrence of reconnection jets at the dayside magnetopause: Double Star observations. *Journal of Geophysical Research*, *113*, A07S10. https://doi.org/10.1029/2007JA012774

Walén, C. (1944). On the Theory of sunspots. *Arkiv för matematik, astronomi och fysik*, *30*, 1–87.

Young, D. T., Burch, J. L., Gomez, R. G., De Los Santos, A., Miller, G. P., Wilson, P., & Webster, J. M. (2016). Hot plasma composition analyzer for the Magnetospheric Multiscale Mission. *Space Science Reviews*, *199*, 407–470. https://doi.org/10.1007/s11214-014-0119-6